IEEE Access
Multidisciplinary ⋮ Rapid Review ⋮ Open Access Journal

Received 20 August 2023, accepted 31 August 2023, date of publication 5 September 2023, date of current version 11 September 2023.

Digital Object Identifier 10.1109/ACCESS.2023.3312175

RESEARCH ARTICLE

Disturbance Observer-Based Frequency Regulation for Shipboard Microgrid With Communication Delay

SHI-TAO RUAN
Department of Automation, Shanghai Jiao Tong University, Shanghai 200240, China
e-mail: struan@sjtu.edu.cn

This work was supported in part by the Hainan Province Science and Technology Special Fund under Grant ZDYF2021GXJS041, in part by the National Key Research and Development Program of China under Grant 2022ZD0119900, in part by the Shanghai Science and Technology Program under Grant 22015810300, and in part by the National Natural Science Foundation of China under Grant U2141234.

ABSTRACT Load frequency control of power systems is inherently a disturbance rejection issue. This paper proposes a disturbance observer-based frequency regulation approach for a shipboard microgrid system with communication delay. The proposed control method consists of the design of both disturbance observer and load frequency controller. The design of disturbance observer involves the acquisition of nominal model and the tuning of Q-filter. The nominal model is obtained via the complex curve fitting technique. Whereas the load frequency controller is designed by the frequency response model matching approach. The maximum sensitivity index is utilized as a robustness specification to tune both Q-filter and load frequency controller. The advantage of the proposed method is that inverse response process dynamics are considered into disturbance observer design to obtain better modeling accuracy and frequency regulation performance. Simulation examples including comparison with classical methods are presented to demonstrate the effectiveness of the proposed method.

INDEX TERMS Disturbance observer, load frequency control, shipboard microgrid, complex curve fitting, frequency response model matching.

I. INTRODUCTION

Marine electrical power systems or shipboard microgrids (MGs) are important components of marine vessels. People use shipboard MGs to reduce environmental pollution and prevent global warming, given that distributed energy resources can be more environmentally friendly than conventional power systems. The development of shipboard MGs coincides with the aim of International Maritime Organization (IMO) by reducing greenhouse gas emissions by 50% by 2050 to satisfy the climate targets of the Paris Agreement [1].

Generally, shipboard MGs with wind turbine (WTG), photovoltaic (PV), energy storage systems (ESSs), and fuel cell (FC) can be regarded as islanded MGs. Over the years, numerous investigations have been conducted on using islanded MGs in marine vessels. In [2], a new intelligent interval type-2 fuzzy logic controller on the basis of sliding mode control is presented for the DC/DC converters in a shipboard MG. In [3], a hybrid PV/diesel system with ESS units is constructed to reduce the cost and environmental pollution. In [4], the stability of a hybrid diesel/PV/battery power system is studied. In [5], production-demand coordination is conducted considering the PV production uncertainties in a shipboard MG. In [6], a multi-objective optimization is carried out for energy management of ESSs in a shipboard MG. Nevertheless, load frequency control (LFC) is not considered in [2], [3], [4], [5], and [6], which plays a critical role in shipboard MGs.

The LFC of MGs aims at realizing the balance between generation and demand under variations of renewable energy sources (RESs) and loads. In [7], a new approach for LFC of a shipboard MG is proposed. In [8], robust mixed μ-synthesis

The associate editor coordinating the review of this manuscript and approving it for publication was Qi Zhou.

based controller is presented for LFC of a shipboard MG. In [9], interval type-2 FOFPD/FPI controller is performed for LFC of a shipboard MG. In [10], Kalman filter is utilized for LFC of a shipboard MG. In [9] and [11], the LFC is performed for a shipboard MG system with communication delay. Recently, new design of LFC is proposed for a shipboard MG including wave energy conversion systems [12]. In [13], a novel LFC method is utilized for a shipboard MG with communication delay via the linear matrix inequality technique. In [14], delay-dependent stability analysis is presented for a shipboard MG.

LFC of microgrids is essentially a disturbance rejection issue. In this regard, disturbance observer is desirable to achieve fast frequency regulation. In [15], a novel coordinated control method is presented to improve the dynamic stability of an isolated wind-diesel hybrid power system via adaptive sliding mode control and disturbance observer. In [16], LFC is designed using adaptive law and disturbance observer for an isolated MG. In [17], the sliding mode LFC is proposed for a hybrid power system through disturbance observer. In [18], decentralized LMI-based event-triggered LFC is designed for power systems with disturbance observer. In [19], a disturbance observer method is proposed for a low-inertia MG system with various distributed energy resources. In [20], a disturbance observer-based control approach is presented for frequency regulation of an MG system consisting of diesel generator and solar PV. In [21], observer-based dynamic event-triggered control is presented for multiagent systems with time-varying delay. However, none of the above methods consider disturbance observer-based LFC design for shipboard MGs.

In this paper, a disturbance observer-based approach is proposed for frequency regulation of a shipboard MG with communication delay. The control system block consists of the design of both disturbance observer and load frequency controller. The design of disturbance observer consists of reduction of nominal model [22], [23], [24] and the Q-filter design. The load frequency controller is designed utilizing the frequency response model matching approach [25], [26], [27].

The motivation of this paper is to propose a method that significantly improves frequency regulation performance. The contributions of the proposed method are as follows:

(1) Disturbance observer-based control is proposed for a shipboard MG with communication delay, compared with the existing methods which do not involve the disturbance observer system [12], [13], [14].
(2) The nominal model of disturbance observer is obtained via the complex curve fitting technique. The Q-filter is designed by satisfying the maximum sensitivity index. On the other hand, the load frequency controller is designed through the frequency response model matching approach.
(3) The proposed disturbance observer-based control utilizes inverse response process dynamics to improve frequency regulation performance, compared with the existing methods [19], [20] which do not involve inverse dynamics.
(4) Real-world wind power and solar radiation data are utilized to verify the effectiveness of the proposed method.

The rest of the paper is organized as follows. Section II focuses on design of disturbance observer. The design of load frequency controller is conducted in Section III. Simulation examples are shown in Section IV. Conclusion is performed in Section V.

II. FREQUENCY REGULATION VIA DISTURBANCE OBSERVER

A. ACQUISITION OF NOMINAL MODEL

The control diagram of the shipboard MG is shown in Figure 1, where $G_g = 1/\left(T_g s+1\right)$, $G_d = 1/\left(T_d s+1\right)$, $G_{FC} = 1/\left(T_{FC} s+1\right)$, $G_{inv1} = 1/\left(T_{inv1} s+1\right)$, $G_{filt1} = 1/\left(T_{filt1} s+1\right)$, $G_{WTG} = 1/\left(T_{WTG} s+1\right)$, $G_{PV} = 1/\left(T_{PV} s+1\right)$, $G_{inv2} = 1/\left(T_{inv2} s+1\right)$, $G_{filt2} = 1/\left(T_{filt2} s+1\right)$, $G_p = 1/\left(Ms+D\right)$, $G_{FE} = 1/\left(T_{FESS} s+1\right)$, $G_{BE} = 1/\left(T_{BESS} s+1\right)$, C is load frequency controller, c(s) is the controller output of C, u(s) is the control input, Δf is frequency deviation, Q is the low-pass filter of disturbance observer, $e^{-\tau s}$ is communication delay, G_{n+} and G_{n-} are non-minimum phase and minimum phase parts of nominal model, respectively. The system parameters of the control scheme is shown in Table 1.

As shown in Fig. 1, define $G_{DEG} = 1/\left(T_g s+1\right)/\left(T_d s+1\right)$, $\tilde{G}_{FC} = 1/\left(T_{FC} s+1\right)/\left(T_{inv1} s+1\right)/\left(T_{filt1} s+1\right)$, $G_P = 1/\left(Ms+D\right)$, $G_{FE} = 1/\left(T_{FESS} s+1\right)$, and $G_{BE} = 1/\left(T_{BESS} s+1\right)$. DOB nominal model can be obtained as

$$G(s) = \frac{\left(G_{DEG}+\tilde{G}_{FC}\right)G_P}{1+\left(G_{DEG}/R+\tilde{G}_{FC}\Big/R+G_{FE}+G_{BE}\right)G_P} \quad (1)$$

Substituting the system parameters in Table 1 into (1), one obtains

$$G(s) = \frac{\begin{array}{l} 9.968\times10^{-13}s^{11}+1.358\times10^{-9}s^{10}+3.642\times10^{-7}s^{9} \\ +2.465\times10^{-5}s^{8}+0.00077s^{7}+0.01326s^{6}+0.1343s^{5} \\ +0.808s^{4}+2.798s^{3}+5.119s^{2}+3.897s+0.216 \end{array}}{\begin{array}{l} 6.38\times10^{-15}s^{14}+3.878\times10^{-12}s^{13}+7.746\times10^{-10}s^{12} \\ +5.982\times10^{-8}s^{11}+2.439\times10^{-6}s^{10}+6.102\times10^{-5}s^{9} \\ +0.001019s^{8}+0.01194s^{7}+0.09966s^{6}+0.5853s^{5} \\ +2.325s^{4}+5.861s^{3}+8.398s^{2}+5.305s+0.2893 \end{array}} \quad (2)$$

Note that the original DOB model is of high order. This poses significant challenges for engineering implementation of the DOB system. Hence, high accuracy low-order model (or nominal model) is desirable to design and implement the DOB loop. The complex curve fitting technique is utilized here to obtain the expression of low-order model.

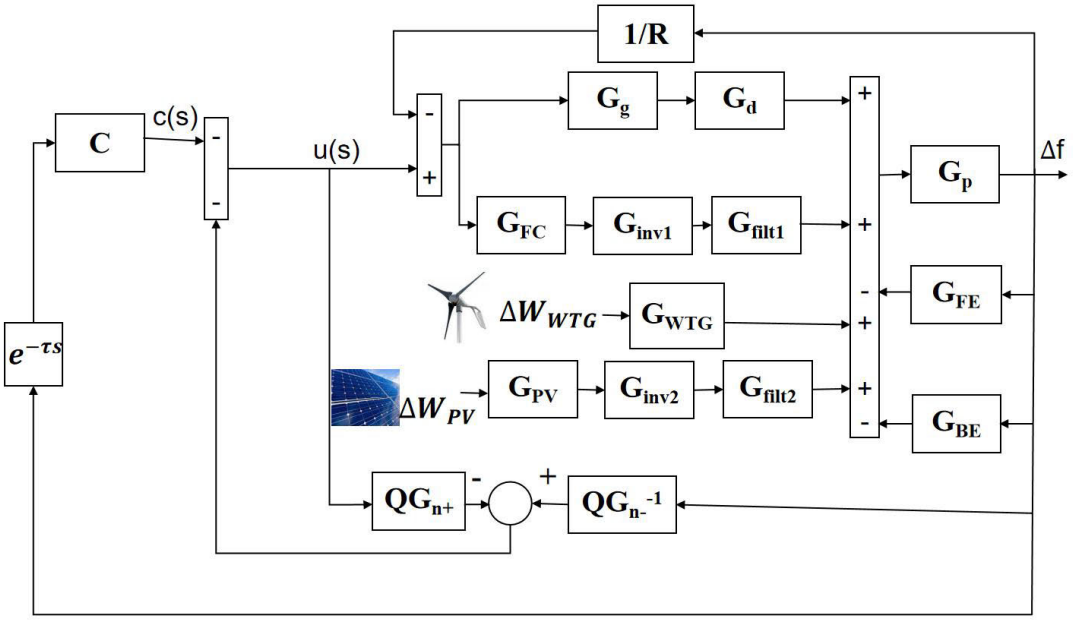

FIGURE 1. The LFC scheme of a shipboard MG system.

TABLE 1. Shipboard microgrid system parameters.

Symbol	Nomenclatures	Values [a]
R	frequency droop coefficient	3
T_g, T_d	diesel generator governor and turbine time constants	0.08, 0.4
$T_{FC}, T_{inv1}, T_{filt1}$	FC, inverter, and interconnection time constants	0.26, 0.04, 0.004
T_{WTG}	time constant of WTG	1.5
$T_{FC}, T_{inv2}, T_{filt2}$	PV, inverter, and interconnection time constants	1.8, 0.04, 0.004
T_{FESS}, T_{BESS}	time constants of FESS and BESS	0.1, 0.1
M, D	equivalent inertia and damping constants	0.2, 0.012

Desired structure of the nominal model is selected as:

$$G_n(s) = \frac{b_2 s^2 + b_1 s + b_0}{a_3 s^3 + a_2 s^2 + a_1 s + 1} \tag{3}$$

where $b_0 = G(0)$. The frequency response of $G_n(s)$ at frequency ω_k is given as

$$G_n(j\omega_k) = \frac{b_0 - b_2\omega_k^2 + jb_1\omega_k}{1 - a_2\omega_k^2 + j(a_1\omega_k - a_3\omega_k^3)} = \frac{\alpha_k + j\beta_k}{\delta_k + j\tau_k} \tag{4}$$

where $\alpha_k = b_0 - b_2\omega_k^2$, $\beta_k = b_1\omega_k$, $\delta_k = 1 - a_2\omega_k^2$, and $\tau_k = a_1\omega_k - a_3\omega_k^3$.

The numerical difference between $G(j\omega_k)$ and $G_n(j\omega_k)$ is defined as

$$e_k = G(j\omega_k) - \frac{\alpha_k + j\beta_k}{\delta_k + j\tau_k} \tag{5}$$

Multiplying both sides of (5) by $\delta_k + j\tau_k$ gives

$$(\delta_k + j\tau_k)\, e_k = G(j\omega_k)(\delta_k + j\tau_k) - \alpha_k - j\beta_k \tag{6}$$

Decompose $G(j\omega_k)$ into $G(j\omega_k) = \mathrm{Re}G_k + \mathrm{Im}G_k$, summing $(\delta_k + j\tau_k)\, e_k$ over the sampling frequency ω_k, the error function E is defined as

$$\begin{aligned} E &= \sum_{k=1}^{L} |(\delta_k + j\tau_k)\, e_k|^2 \\ &= \sum_{k=1}^{L} \left[\begin{array}{l} (ReG_k\delta_k - ImG_k\tau_k - \alpha_k)^2 \\ + (ReG_k\tau_k + ImG_k\delta_k - \beta_k)^2 \end{array} \right] \end{aligned} \tag{7}$$

By differentiating (7) with respect to a_u and b_v and setting the results equal to zero, we get

$$\frac{\partial E}{\partial a_u} = \sum_{k=1}^{L} \left[\begin{array}{l} (ReG_k\delta_k - ImG_k\tau_k - \alpha_k) \\ \left(ReG_k \dfrac{\partial \delta_k}{\partial a_u} - ImG_k \dfrac{\partial \tau_k}{\partial a_u} \right) \\ + (ReG_k\tau_k + ImG_k\delta_k - \beta_k) \\ \left(ReG_k \dfrac{\partial \tau_k}{\partial a_u} + ImG_k \dfrac{\partial \delta_k}{\partial a_u} \right) \end{array} \right] = 0 \tag{8}$$

$$\frac{\partial E}{\partial b_v} = \sum_{k=1}^{L} \left[\begin{array}{l} (ReG_k\delta_k - ImG_k\tau_k - \alpha_k) \dfrac{-\partial \alpha_k}{\partial b_v} \\ + (ReG_k\tau_k + ImG_k\delta_k - \beta_k) \dfrac{-\partial \beta_k}{\partial b_v} \end{array} \right] = 0 \tag{9}$$

It is obtained from (4) that

$$\begin{aligned} \frac{\partial \beta_k}{\partial b_1} = \omega_k, \quad \frac{\partial \alpha_k}{\partial b_2} = -\omega_k^2, \quad \frac{\partial \tau_k}{\partial a_1} = \omega_k, \quad \frac{\partial \tau_k}{\partial a_3} \\ = -\omega_k^3, \quad \frac{\partial \delta_k}{\partial a_2} = -\omega_k^2 \end{aligned} \tag{10}$$

Substituting (4) and (10) into (8) and (9) yields

$$\begin{bmatrix} b_1 \\ b_2 \\ a_1 \\ a_2 \\ a_3 \end{bmatrix} = \begin{bmatrix} \Delta_{11} & \Delta_{12} & \Delta_{13} & \Delta_{14} & \Delta_{15} \\ \Delta_{21} & \Delta_{22} & \Delta_{23} & \Delta_{24} & \Delta_{25} \\ \Delta_{31} & \Delta_{32} & \Delta_{33} & \Delta_{34} & \Delta_{35} \\ \Delta_{41} & \Delta_{42} & \Delta_{43} & \Delta_{44} & \Delta_{45} \\ \Delta_{51} & \Delta_{52} & \Delta_{53} & \Delta_{54} & \Delta_{55} \end{bmatrix}^{-1} \begin{bmatrix} \varphi_1 \\ \varphi_2 \\ \varphi_3 \\ \varphi_4 \\ \varphi_5 \end{bmatrix} \tag{11}$$

where $\Delta_{11} = \sum_{k=1}^{L} \left(\mathrm{Re}G_k\omega_k^2\right)$, $\Delta_{12} = \sum_{k=1}^{L} \left(\mathrm{Im}G_k\omega_k^3\right)$, $\Delta_{13} = -\sum_{k=1}^{L} \left(\left|G_k\right|^2 \omega_k^2\right)$, $\Delta_{14} = 0$, $\Delta_{15} = \sum_{k=1}^{L} \left(\left|G_k\right|^2\omega_k^4\right)$, $\Delta_{21} = \sum_{k=1}^{L} \left(\mathrm{Im}G_k\omega_k^3\right)$, $\Delta_{22} = -\sum_{k=1}^{L} \left(\mathrm{Re}G_k\omega_k^4\right)$, $\Delta_{23} = 0$, $\Delta_{24} = \sum_{k=1}^{L} \left(\left|G_k\right|^2\omega_k^4\right)$, $\Delta_{25} = 0$, $\Delta_{31} = \sum_{k=1}^{L} \left(\mathrm{Re}G_k\omega_k^4\right)$, $\Delta_{32} = \sum_{k=1}^{L} \left(\mathrm{Im}G_k\omega_k^5\right)$, $\Delta_{33} = -\sum_{k=1}^{L} \left(\left|G_k\right|^2\omega_k^4\right)$, $\Delta_{34} = 0$, $\Delta_{35} = \sum_{k=1}^{L} \left(\left|G_k\right|^2\omega_k^6\right)$, $\Delta_{41} = \sum_{k=1}^{L} \omega_k$, $\Delta_{42} = 0$, $\Delta_{43} = -\sum_{k=1}^{L} \left(\mathrm{Re}G_k\omega_k\right)$, $\Delta_{44} = \sum_{k=1}^{L} \left(\mathrm{Im}G_k\omega_k^2\right)$, $\Delta_{45} = \sum_{k=1}^{L} \left(\mathrm{Re}G_k\omega_k^3\right)$, $\Delta_{51} = 0$, $\Delta_{52} = \sum_{k=1}^{L} \omega_k^4$, $\Delta_{53} = -\sum_{k=1}^{L} \left(\mathrm{Im}G_k\omega_k^3\right)$, $\Delta_{54} = -\sum_{k=1}^{L} \left(\mathrm{Re}G_k\omega_k^4\right)$, $\Delta_{55} = \sum_{k=1}^{L} \left(\mathrm{Im}G_k\omega_k^5\right)$, $\varphi_1 = \sum_{k=1}^{L} \left(b_0\mathrm{Im}G_k\omega_k\right)$, $\varphi_2 = \sum_{k=1}^{L} \left(\left|G_k\right|^2\omega_k^2 - b_0\mathrm{Re}G_k\right)$, $\varphi_3 = \sum_{k=1}^{L} \left(b_0\mathrm{Im}G_k\omega_k^3\right)$, $\varphi_4 = \sum_{k=1}^{L} \mathrm{Im}G_k$, $\varphi_5 = \sum_{k=1}^{L} \left[\omega_k^2\left(b_0 - \mathrm{Re}G_k\right)\right]$.

Let $L = 30$ and ω_L be the ultimate frequency of $G(s)$ ($\omega_L = 13.4724$ in this work). The nominal model $G_n(s)$ is obtained from (11) as

$$G_n(s) = \frac{-0.0007s^2 + 0.0216s + 0.7466}{0.0023s^3 + 0.0289s^2 + 0.3177s + 1} \tag{12}$$

To design the DOB system, $\mathrm{G_n}(s)$ is decomposed into $G_n(s) = G_{n+}(s)\,G_{n-}(s)$, where $G_{n+}(s) = -0.0194s + 1$, $G_{n-}(s) = 0.7466(0.0483s + 1)/(0.0023s^3 + 0.0289s^2 + 0.3177s + 1)$.

Note that inverse response process dynamics $G_{n+}(s)$ have been considered into disturbance observer design to improve frequency regulation performance, compared with the existing methods [19], [20] which do not involve inverse dynamics.

B. DESIGN OF Q-FILTER

It is obtained from Fig. 1 that $\Delta f(s) = G(s)u(s)$ and $G(s) \approx \mathrm{G_n}(s) = G_{n+}(s)\,G_{n-}(s)$. Hence, we have

$$\begin{aligned} u(s) &= -c(s) - \left[G_{n-}^{-1}(s)\,Q(s)\,\Delta f(s) - G_{n+}(s)Q(s)u(s)\right] \\ &= -c(s) - Q(s)\left[G_{n-}^{-1}(s)\,G(s)\,u(s) - G_{n+}(s)\,u(s)\right] \\ &\approx -\mathrm{c}(s) - \mathrm{Q}(s)\left[\mathrm{G}_{\mathrm{n}-}^{-1}(s)\,\mathrm{G_n}(s)\mathrm{u}(s) - \mathrm{G}_{\mathrm{n}+}(s)\mathrm{u}(s)\right] \\ &= -\mathrm{c}(s) \end{aligned} \tag{13}$$

The above expression means that the load frequency controller C and the Q-filter can be designed independently from each other. To guarantee the properness of the DOB system and to compromise between system performance and robustness, the Q-filter is chosen as

$$Q(s) = \frac{1}{(\lambda s + 1)^2} \tag{14}$$

The open-loop transfer function of the DOB system is

$$G_L(s) = \frac{Q(s)G_{n+}(s)}{1 + Q(s)G_{n+}(s)} \tag{15}$$

The parameter λ in Q(s) is evaluated by satisfying the desired closed-loop system robustness in terms of

$$M_s = \left|\frac{1}{1 + G_L(j\omega)}\right| \tag{16}$$

III. DESIGN OF LOAD FREQUENCY CONTROLLER

To obtain satisfactory frequency regulation performance, define the desired closed-loop transfer function as

$$\tilde{T}(s) = \frac{(\gamma s + 1)\,e^{-\tau s}}{\left(\tau_c s^2 + 2\xi\tau_c s + 1\right)(\tau_c s + 1)} \tag{17}$$

where γ and ξ are adjustable parameters for the user to specify, τ_c is utilized to achieve the desired robustness of the closed-loop system.

The desired open-loop transfer function is obtained from (17) as

$$G_r(s) = \frac{\tilde{T}(s)}{1 - \tilde{T}(s)} \tag{18}$$

The load frequency controller is defined as a practical PID controller:

$$C(s) = \frac{a_2 s^2 + a_1 s + 1}{b_2 s^2 + b_1 s} \tag{19}$$

Define $\tilde{G}(s) = G(s)\mathrm{e}^{-\tau s}$ and $\theta = [a_2; a_1; b_2; b_1]$, the design of load frequency controller is equivalent to minimize

$$\min_{\theta} \sum_{i=1}^{N} \left|C(j\omega_i)\,\tilde{G}(j\omega_i) - G_r(j\omega_i)\right|^2 \tag{20}$$

Substituting (19) into (20) gives

$$\min_{\theta} \sum_{i=1}^{N} \left|-a_2\omega_i^2\tilde{G} + a_1 j\omega_i\tilde{G} + b_2\omega_i^2 G_r - b_1 j\omega_i G_r + \tilde{G}\right|^2 \tag{21}$$

The design problem is then simplified to

$$\min_{\theta} \|\Psi\theta - \Omega\|^2 \tag{22}$$

where

$$\Psi = \begin{bmatrix} -\omega_1^2\tilde{G}(j\omega_1) & j\omega_1\tilde{G}(j\omega_1) & \omega_1^2 G_r(j\omega_1) & -j\omega_1 G_r(j\omega_1) \\ -\omega_2^2\tilde{G}(j\omega_2) & j\omega_2\tilde{G}(j\omega_2) & \omega_2^2 G_r(j\omega_2) & -j\omega_2 G_r(j\omega_2) \\ \vdots & \vdots & \vdots & \vdots \\ -\omega_N^2\tilde{G}(j\omega_N) & j\omega_N\tilde{G}(j\omega_N) & \omega_N^2 G_r(j\omega_N) & -j\omega_N G_r(j\omega_N) \end{bmatrix}$$

$$\Omega = \left[-G(j\omega_1) - G(j\omega_2) \cdots - G(j\omega_N)\right]^T$$

Define $\Psi' = [\mathrm{Re}(\Psi); \mathrm{Im}(\Psi)]$ and $\Omega' = [\mathrm{Re}(\Omega); \mathrm{Im}(\Omega)]$, (22) is then equivalent to

$$\min_{\theta} \left\|\Psi'\theta - \Omega'\right\|^2 \tag{23}$$

which can be solved through the standard least squares method as

$$\theta^* = \left(\Psi'^T \Psi'\right)^{-1} \Psi'^T \Omega' \tag{24}$$

Note that Ψ is non-singular. Hence, it can be easily derived that $\Psi'^T \Psi'$ satisfy the condition of non-singularity. Equation (24) gives the optimal PID settings as $a_2 = \theta^*(1)$, $a_1 = \theta^*(2)$, $b_2 = \theta^*(3)$, and $b_1 = \theta^*(4)$.

Note that θ^* is a function of τ_c, which is adjusted by satisfying the desired closed-loop system robustness evaluated by

$$M_s = \max_{\omega \in [0,+\infty)} \left| \frac{1}{1 + C(j\omega)\tilde{G}(j\omega)} \right| \tag{25}$$

IV. SIMULATION EXAMPLES

The effectiveness of the proposed method is tested through four illustrative examples. In the first example, the load frequency control performance is evaluated. In the second example, the effectiveness of the proposed disturbance observer with inverse response dynamics is verified. In the third example, the improved control performance via disturbance observer is demonstrated. In the fourth example, the real-world wind power and solar radiation data are utilized to verify the effectiveness of the proposed method.

A. EVALUATION OF LOAD FREQUENCY CONTROLLER

The load frequency control performance is evaluated without the participation of the DOB system. The adjustable parameters in $\tilde{T}(s)$ are chosen as $\gamma = 1$ and $\xi = 1.1$. To achieve different desired system robustness, τ_c is chosen as 0.5, 0.7, and 0.9, respectively. The corresponding control parameters are computed as $a_2 = 0.2476$, $a_1 = 0.9029$, $b_2 = 0.4376$, $b_1 = 1.1897$ for $\tau_c = 0.5$, $a_2 = -0.0587$, $a_1 = 0.3875$, $b_2 = 0.0095$, $b_1 = 1.6779$ for $\tau_c = 0.7$, and $a_2 = -0.0170$, $a_1 = 0.5320$, $b_2 = 0.6688$, $b_1 = 2.1559$ for $\tau_c = 0.9$.

The control performance is compared with the method proposed by Yildirim [12], whose controller structure is a conventional PI form with parameters chosen as $K_P = 0.4$ and $K_I = 0.75$ to achieve the desired system robustness evaluated by gain and phase margins. The frequency response results under load disturbance of $\Delta P_L = 0.1$ are shown in Fig. 2.

It is shown that the proposed method is flexible in that an explicit trade-off between system performance and robustness can be achieved. Increasing τ_c slows down the response speed of frequency regulation, but the control signal gets more smooth. Decreasing τ_c speeds up frequency regulation performance, at the expense of more aggressive control signal.

B. VERIFICATION OF INVERSE RESPONSE PROCESS DYNAMICS

The effectiveness of the proposed disturbance observer structure with inverse response process dynamics is verified in this Section. The filter time constant is chosen as 0.05. The frequency response results under load disturbance of $\Delta P_L = 0.1$ with and without inverse response process dynamics are shown in Fig. 3.

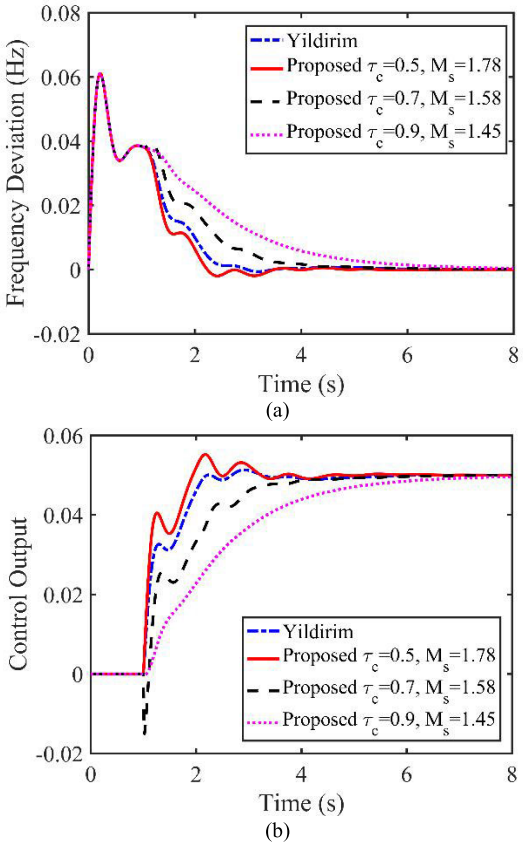

FIGURE 2. Comparison of load frequency control performance without the DOB system.

It is shown that similar frequency regulation performance can be obtained by both methods. However, the control signal is significantly less aggressive by disturbance observer with inverse response dynamics.

C. EVALUATION OF DISTURBANCE OBSERVER

The proposed method with disturbance observer is compared with Yildirim's method [12]. The parameter τ_c is fixed as 0.5. The DOB filter time constant is chosen as 0.03, 0.04, and 0.05, which satisfies the desired robustness with M_s =2.11, 1.61, and 1.44, respectively. The frequency response results under load disturbance of $\Delta P_L = 0.1$ are shown in Fig. 4.

It is shown that significantly better performance can be obtained by the proposed method with disturbance observer. Yildirim's method gives sluggish response speed, whose control signal acts after the communication delay. Whereas the disturbance observer takes actions before the communication delay, which is responsible for faster frequency regulation performance.

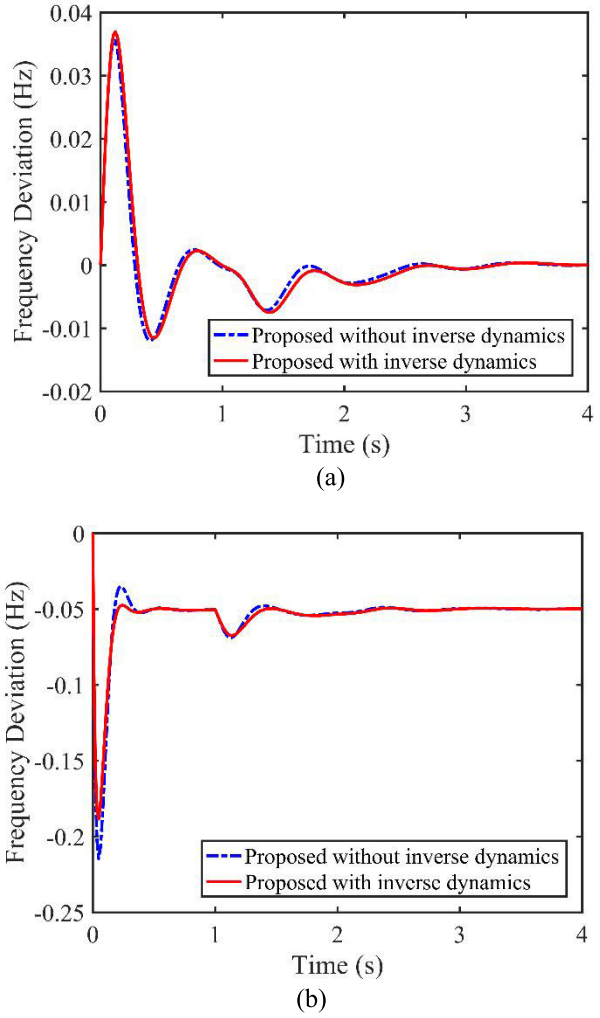

FIGURE 3. Verification of inverse response process dynamics.

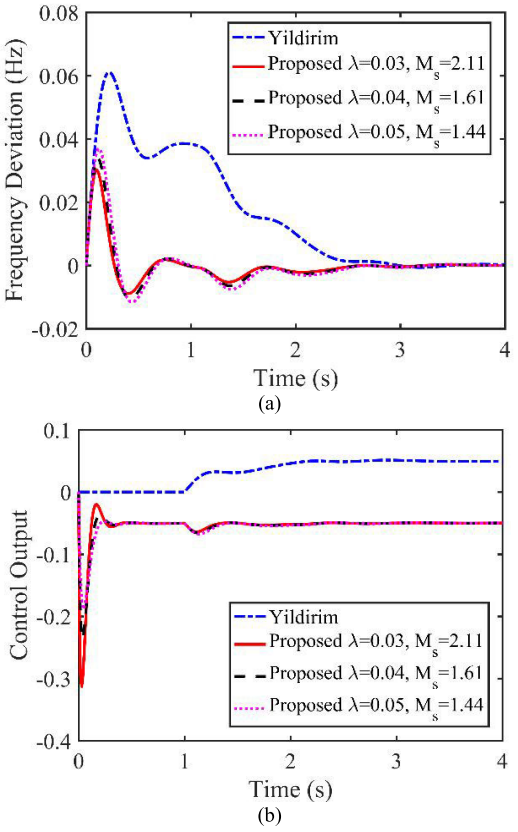

FIGURE 4. Comparison of frequency regulation performance with the DOB system.

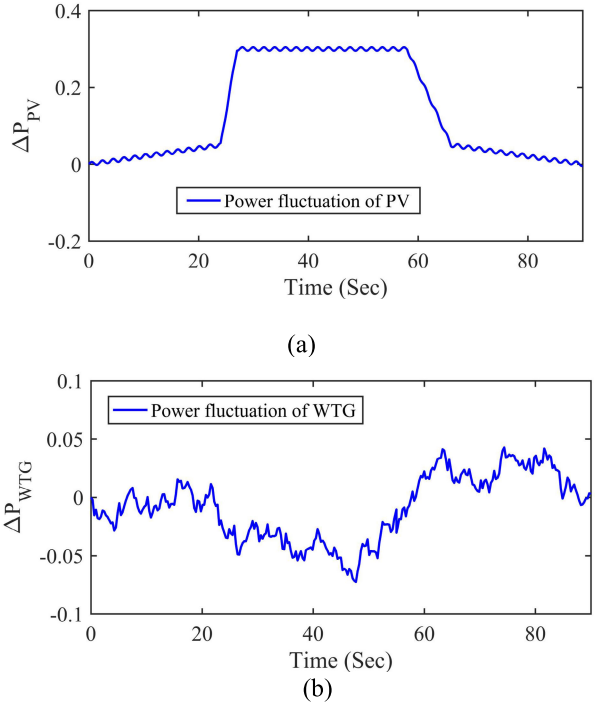

FIGURE 5. Power fluctuations of: (a) PV [7]. (b) Wind turbine generator.

D. EVALUATION UNDER REAL-WORLD WIND POWER AND SOLAR RADIATION DATA

The real-world solar radiation and wind power fluctuation data are used to verify the effectiveness of the proposed method. The solar radiation data are utilized from Aberdeen (United Kingdom) [7], whereas the wind powe ***r***fluctuation data are obtained from the National Renewable Energy Laboratory (NREL) [28]. The power fluctuations of PV and WTG are shown in Fig. 5.

The proposed disturbance observer-based control is compared with Yildirim's method [12]. The parameter τ_c is fixed as 0.5. The DOB filter time constant is chosen as 0.05, which satisfies the desired robustness with M_s =1.44. The frequency response results under real-world solar radiation and wind power fluctuation data are shown in Fig. 6.

It is shown that significantly better performance can be obtained by the proposed method. Yildirim's method gives very large response peak values. The proposed method yields opposite compensation signals of wind power and solar radiation data, which helps give faster frequency regulation performance.

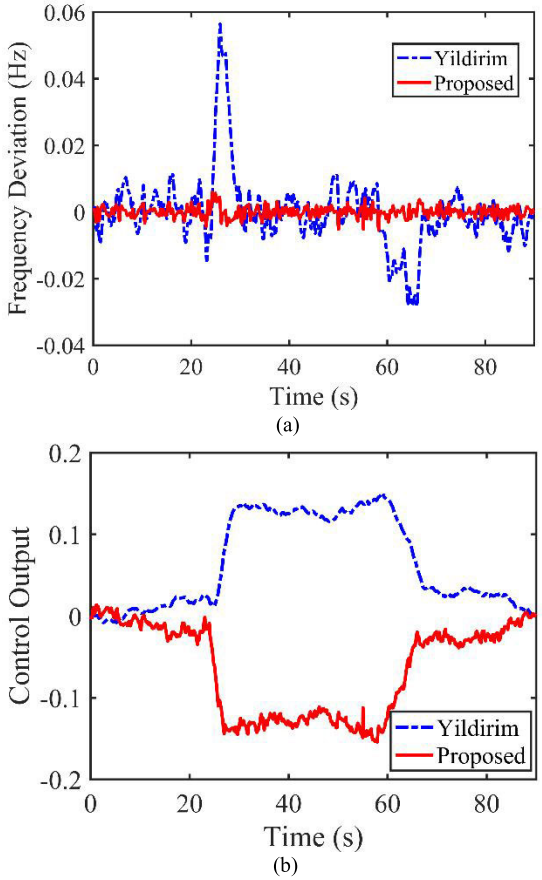

FIGURE 6. Comparison of frequency regulation performance under power fluctuations of PV and wind turbine generator.

V. CONCLUSION

In this paper, the disturbance observer-based control approach has been proposed for a shipboard microgrid system with communication delay. Control system design consists of the design of both disturbance observer and load frequency controller. The disturbance observer is designed via the complex curve fitting technique. On the other hand, the load frequency controller is designed through the frequency response model matching approach. The proposed disturbance observer-based control approach has the advantage that process inverse response dynamics have been considered into the design to improve frequency regulation performance. Simulation results show that significant better performance can be obtained by the proposed method than the existing methods. Future work aims at disturbance observer-based control for multi-area microgrids with communication delay.

REFERENCES

[1] (2023). *International Shipping*. Accessed: May 16, 2023. [Online]. Available: https://www.iea.org/reports/international-shipping

[2] M. H. Khooban, M. Gheisarnejad, H. Farsizadeh, A. Masoudian, and J. Boudjadar, "A new intelligent hybrid control approach for DC–DC converters in zero-emission ferry ships," *IEEE Trans. Power Electron.*, vol. 35, no. 6, pp. 5832–5841, Jun. 2020.

[3] A. Maleki and A. Askarzadeh, "Artificial bee swarm optimization for optimum sizing of a stand-alone PV/WT/FC hybrid system considering LPSP concept," *Sol. Energy*, vol. 107, pp. 227–235, Sep. 2014.

[4] Z. Jin, G. Sulligoi, R. Cuzner, L. Meng, J. C. Vasquez, and J. M. Guerrero, "Next-generation shipboard DC power system: Introduction smart grid and DC microgrid technologies into maritime electrical networks," *IEEE Electrific. Mag.*, vol. 4, no. 2, pp. 45–57, Jun. 2016.

[5] S. Fang, Y. Xu, S. Wen, T. Zhao, H. Wang, and L. Liu, "Data-driven robust coordination of generation and demand-side in photovoltaic integrated all-electric ship microgrids," *IEEE Trans. Power Syst.*, vol. 35, no. 3, pp. 1783–1795, May 2020.

[6] S. Fang, Y. Xu, Z. Li, T. Zhao, and H. Wang, "Two-step multi-objective management of hybrid energy storage system in all-electric ship microgrids," *IEEE Trans. Veh. Technol.*, vol. 68, no. 4, pp. 3361–3373, Apr. 2019.

[7] M.-H. Khooban, T. Dragicevic, F. Blaabjerg, and M. Delimar, "Shipboard microgrids: A novel approach to load frequency control," *IEEE Trans. Sustain. Energy*, vol. 9, no. 2, pp. 843–852, Apr. 2018.

[8] K. Torabi-Farsani, M. H. Asemani, F. Badfar, N. Vafamand, and M. H. Khooban, "Robust mixed μ-synthesis frequency regulation in AC mobile power grids," *IEEE Trans. Transport. Electrific.*, vol. 5, no. 4, pp. 1182–1189, Dec. 2019.

[9] M. Gheisarnejad, M.-H. Khooban, and T. Dragicevié, "The future 5G network-based secondary load frequency control in shipboard microgrids," *IEEE J. Emerg. Sel. Topics Power Electron.*, vol. 8, no. 1, pp. 836–844, Mar. 2020.

[10] S. Yousefizadeh, J. D. Bendtsen, N. Vafamand, M. H. Khooban, T. Dragicevic, and F. Blaabjerg, "EKF-based predictive stabilization of shipboard DC microgrids with uncertain time-varying load," *IEEE J. Emerg. Sel. Topics Power Electron.*, vol. 7, no. 2, pp. 901–909, Jun. 2019.

[11] M. H. Khooban, N. Vafamand, T. Dragicevic, M. M. Mardani, and R. Heydari, "Modeling and HiL real-time simulation for the secondary LFC in time-delay shipboard microgrids," in *Proc. IEEE Int. Conf. Electr. Syst. Aircr., Railway, Ship Propuls. Road Vehicles Int. Transp. Electrific. Conf. (ESARS-ITEC)*, Nov. 2018, pp. 1–5.

[12] B. Yildirim, "Gain and phase margins based stability region analysis of time-delayed shipboard microgrid with sea wave energy," *IET Electric Power Appl.*, vol. 14, no. 8, pp. 1347–1359, Aug. 2020.

[13] N. Vafamand, M. H. Khooban, T. Dragicevic, J. Boudjadar, and M. H. Asemani, "Time-delayed stabilizing secondary load frequency control of shipboard microgrids," *IEEE Syst. J.*, vol. 13, no. 3, pp. 3233–3241, Sep. 2019.

[14] B. Yildirim, M. Gheisarnejad, and M. H. Khooban, "Delay-dependent stability analysis of modern shipboard microgrids," *IEEE Trans. Circuits Syst. I, Reg. Papers*, vol. 68, no. 4, pp. 1693–1705, Apr. 2021.

[15] Y. Mi, Y. Song, Y. Fu, X. Su, C. Wang, and J. Wang, "Frequency and voltage coordinated control for isolated wind-Diesel power system based on adaptive sliding mode and disturbance observer," *IEEE Trans. Sustain. Energy*, vol. 10, no. 4, pp. 2075–2083, Oct. 2019.

[16] C. Wang, Y. Mi, Y. Fu, and P. Wang, "Frequency control of an isolated micro-grid using double sliding mode controllers and disturbance observer," *IEEE Trans. Smart Grid*, vol. 9, no. 2, pp. 923–930, Mar. 2018, doi: 10.1109/TSG.2016.2571439.

[17] Y. Mi, Y. Fu, D. Li, C. Wang, P. C. Loh, and P. Wang, "The sliding mode load frequency control for hybrid power system based on disturbance observer," *Int. J. Electr. Power Energy Syst.*, vol. 74, pp. 446–452, Jan. 2016.

[18] J. Ansari, A. R. Abbasi, and B. B. Firouzi, "Decentralized LMI-based event-triggered integral sliding mode LFC of power systems with disturbance observer," *Int. J. Electr. Power Energy Syst.*, vol. 138, Jun. 2022, Art. no. 107971.

[19] D. Sharma and S. Mishra, "Disturbance-observer-based frequency regulation scheme for low-inertia microgrid systems," *IEEE Syst. J.*, vol. 14, no. 1, pp. 782–792, Mar. 2020.

[20] H. Grover, A. Verma, and T. S. Bhatti, "DOBC-based frequency & voltage regulation strategy for PV-diesel hybrid microgrid during islanding conditions," *Renew. Energy*, vol. 196, pp. 883–900, Aug. 2022.

[21] L. Cao, Y. Pan, H. Liang, and T. Huang, "Observer-based dynamic event-triggered control for multiagent systems with time-varying delay," *IEEE Trans. Cybern.*, vol. 53, no. 5, pp. 3376–3387, May 2023, doi: 10.1109/TCYB.2022.3226873.
[22] W. Yu, Y. Luo, Y. Chen, and Y. Pi, "Frequency domain modelling and control of fractional-order system for permanent magnet synchronous motor velocity servo system," *IET Control Theory Appl.*, vol. 10, no. 2, pp. 136–143, Jan. 2016.
[23] E. C. Levy, "Complex-curve fitting," *IRE Trans. Autom. Control*, vol. AC-4, no. 1, pp. 37–43, May 1959.
[24] S. Saxena, "Load frequency control strategy via fractional-order controller and reduced-order modeling," *Int. J. Electr. Power Energy Syst.*, vol. 104, pp. 603–614, Jan. 2019.
[25] Q.-G. Wang, C.-C. Hang, and Q. Bi, "A frequency domain controller design method," *Chem. Eng. Res. Design*, vol. 75, no. 1, pp. 64–72, Jan. 1997.
[26] J.-C. Jeng and E.-P. Fu, "Closed-loop tuning of set-point-weighted proportional-integral-derivative controllers for stable, integrating, and unstable processes: A unified data-based method," *Ind. Eng. Chem. Res.*, vol. 54, no. 3, pp. 1041–1058, Jan. 2015.
[27] X. Gao, J. Zhang, F. Yang, C. Shang, and D. Huang, "Robust proportional-integral-derivative (PID) design for parameter uncertain second-order plus time delay (SOPTD) processes based on reference model approximation," *Ind. Eng. Chem. Res.*, vol. 56, no. 41, pp. 11903–11918, Oct. 2017.
[28] *Laboratory NRE*. Wind Data. Accessed: May 25, 2023. [Online]. Available: https://www.nrel.gov/grid/eastern-wind-data.html

SHI-TAO RUAN received the B.S. and M.S. degrees from the Shaanxi University of Science and Technology, Xi'an, China, in 2013 and 2016, respectively. He is currently pursuing the Ph.D. degree with the Department of Automation, Shanghai Jiao Tong University, Shanghai, China. His current research interests include shipboard microgrid, renewable energy system power generation, smart grid load frequency control, and power system stability analysis.